4.3 The Double-Couple Solution in an Infinite Homogeneous Medium

This section describes one more step in the sequence of wave solutions that we initiated in Box 4.1 with a scalar wave, spreading in spherically symmetric fashion from a point source. We have seen how to synthesize vector waves and second-order tensor fields G_{ij}. Now we wish to study the third-order tensor field $G_{np,q}$ so that we may understand the radiation pattern (in both near field and far field) for the waves set up by a displacement discontinuity (see (3.18), or, for a point source, (3.23)). We shall conclude with remarkably straightforward formulas (4.32)–(4.33) for the displacement due to a moment tensor **M** corresponding to a point shear dislocation. These formulas describe the far-field radiation pattern that has actually been observed in many thousands of earthquakes. Since this double-couple source is of such practical interest, it might be thought that we should restrict our analysis to a particular combination such as $M_0 * (\partial G_{n1}/\partial \xi_3) + M_0 * (\partial G_{n3}/\partial \xi_1)$ (see (3.23) and (3.25)). Instead, with less effort and using the summation convention we shall work with the fully general nine couples in $M_{pq} * G_{np,q}$.

Our principal findings will be that far-field displacements still attenuate as r^{-1} and are proportional to particle velocity at the source; that certain remarkable similarities are found between far-field and near-field radiation patterns; and that the final static displacement, set up throughout the medium by a displacement dislocation that eventually reaches a final fixed offset, attenuates as r^{-2}.

We start with an application of Stokes' solution, (4.23), to obtain the n-component of displacement due to a body-force distribution $\mathbf{f}(\mathbf{x}, t) = \mathbf{F}(t)\delta(\mathbf{x} - \xi)$, i.e., the force $\mathbf{F}(t)$ applied at ξ. This displacement, at $(\mathbf{x}, t)$, is

$$F_p * G_{np} = \frac{1}{4\pi\rho}(3\gamma_n\gamma_p - \delta_{np})\frac{1}{r^3}\int_{r/\alpha}^{r/\beta} \tau F_p(t-\tau)\,d\tau + \frac{1}{4\pi\rho\alpha^2}\gamma_n\gamma_p\frac{1}{r}F_p\left(t-\frac{r}{\alpha}\right) - \frac{1}{4\pi\rho\beta^2}(\gamma_n\gamma_p - \delta_{np})\frac{1}{r}F_p\left(t-\frac{r}{\beta}\right), \quad (4.27)$$

in which $r = |\mathbf{x} - \xi|$ is the source–receiver distance and direction cosines $\gamma_i = (x_i - \xi_i)/r$ are referred to a source at ξ. Formula (4.27) has the same apparent form as (4.23), but now a summation over p is present, since **F** in general is not along a particular coordinate direction.

In order to obtain the total effect of nine couples, of the type shown in Figure 3.7, we can evaluate (4.27) for $\mathbf{F}(t)$ applied at $\xi + \Delta\mathbf{l}_q$ (where $\Delta\mathbf{l}_q$ is a small distance in the ξ_q-direction) and subtract the value of (4.27) for $\mathbf{F}(t)$ applied at ξ. This difference gives the displacement field (at **x**) due to a couple with the moment $|\Delta l_q|\,|\mathbf{F}|$, and it is a difference which, to first order in Δl_q, is given directly by the calculus operation $\Delta l_q(\partial/\partial\xi_q)$. (This is a dimensionless operation, so the result is still a displacement. The sum over q gives the outcome for all of the three possible "arm" directions.) The final step is to equate the product $\Delta l_q F_p(t)$, in which $\Delta l_q \to 0$ and $F_p \to \infty$ such that the product remains finite, with the moment tensor component $M_{pq}(t)$.

The above procedure is expressed by the equality

$$M_{pq} * G_{np,q} = \begin{pmatrix} \text{limit} \\ {\scriptstyle \Delta l_q \to 0} \\ {\scriptstyle F_p \to \infty} \\ {\scriptstyle \Delta l_q F_p = M_{pq}} \end{pmatrix} \Delta l_q F_p * \frac{\partial}{\partial \xi_q} G_{np}. \tag{4.28}$$

The summation is over both p and q. The operation given in (4.28) is straightforward to apply to (4.27), using the two rules

$$\frac{\partial r}{\partial \xi_q} = -\gamma_q \qquad \text{and} \qquad \frac{\partial \gamma_j}{\partial \xi_q} = \frac{\gamma_j \gamma_q - \delta_{jq}}{r},$$

and the outcome is a displacement field (see (3.23)) having the nth component

$$\begin{aligned} M_{pq} * G_{np,q} = {} & \left(\frac{15\gamma_n\gamma_p\gamma_q - 3\gamma_n\delta_{pq} - 3\gamma_p\delta_{nq} - 3\gamma_q\delta_{np}}{4\pi\rho} \right) \frac{1}{r^4} \int_{r/\alpha}^{r/\beta} \tau M_{pq}(t-\tau)\, d\tau \\ & + \left(\frac{6\gamma_n\gamma_p\gamma_q - \gamma_n\delta_{pq} - \gamma_p\delta_{nq} - \gamma_q\delta_{np}}{4\pi\rho\alpha^2} \right) \frac{1}{r^2} M_{pq}\left(t - \frac{r}{\alpha}\right) \\ & - \left(\frac{6\gamma_n\gamma_p\gamma_q - \gamma_n\delta_{pq} - \gamma_p\delta_{nq} - 2\gamma_q\delta_{np}}{4\pi\rho\beta^2} \right) \frac{1}{r^2} M_{pq}\left(t - \frac{r}{\beta}\right) \\ & + \frac{\gamma_n\gamma_p\gamma_q}{4\pi\rho\alpha^3} \frac{1}{r} \dot{M}_{pq}\left(t - \frac{r}{\alpha}\right) - \left(\frac{\gamma_n\gamma_p - \delta_{np}}{4\pi\rho\beta^3} \right) \gamma_q \frac{1}{r} \dot{M}_{pq}\left(t - \frac{r}{\beta}\right). \end{aligned} \tag{4.29}$$

The near-field terms in this displacement field, radiated by a general second-order symmetric moment tensor (point source), are proportional to $r^{-4} \int_{r/\alpha}^{r/\beta} \tau M_{pq}(t-\tau)\, d\tau$, and the far-field terms are proportional to $r^{-1}\dot{M}_{pq}(t - r/\alpha)$ (P-waves) or to $r^{-1}\dot{M}_{pq}(t - r/\beta)$ (S-waves). Recall from Chapter 3 (equation (3.23)) that $M_{pq} * G_{np,q}$ is the n-component of displacement, at $\mathbf{x}$, from a displacement discontinuity over a fault plane with linear dimensions much smaller than the wavelength of radiated waves of interest at the receiver, so that components of the moment tensor $\mathbf{M}$ are proportional to particle displacements averaged over the fault plane. It follows that $\dot{M}_{pq}(t - r/\alpha)$ and $\dot{M}_{pq}(t - r/\beta)$, giving the pulse shape of displacement in the far field, are proportional to particle *velocities* at the source, averaged over the fault plane.

Present in (4.29) are some terms proportional to $r^{-2}M_{pq}(t - r/\alpha)$ and $r^{-2}M_{pq}(t - r/\beta)$. Since their asymptotic properties, at small and large values of r, are intermediate to the asymptotic properties of the near-field and far-field displacements, we can naturally call these the *intermediate-field terms*. This is, however, a slightly misleading name, since there is no intermediate range of distances in which these terms dominate, so it is common to include them with the near-field terms. Vidale *et al.* (1995) pointed out an unusual example where an effect of these intermediate terms is observable at great distance from a very large deep earthquake (see also Problem 4.11).

From the generality of formula (4.29), which gives the radiation from any moment tensor $\mathbf{M}$, we shall often specialize to cases where $\mathbf{M}$ arises from a shear dislocation. The averaged displacement discontinuity, $\bar{\mathbf{u}}$, is then parallel to the fault surface: $\bar{\mathbf{u}} \cdot \boldsymbol{\nu} = 0$, where $\boldsymbol{\nu}$ is normal to the fault surface. And from (3.24) and (3.21), we see that $M_{pq} = \mu(\bar{u}_p \nu_q + \bar{u}_q \nu_p)A$ for a fault with area A. Then

$$
\begin{aligned}
&\mu(\bar{u}_p \nu_q + \bar{u}_q \nu_p)A * G_{np,q} \\
&= \left(\frac{30\gamma_n\gamma_p\gamma_q\nu_q - 6\nu_n\gamma_p - 6\delta_{np}\gamma_q\nu_q}{4\pi\rho r^4}\right)\mu A \int_{r/\alpha}^{r/\beta} \tau \bar{u}_p(t-\tau)\,d\tau \\
&\quad + \left(\frac{12\gamma_n\gamma_p\gamma_q\nu_q - 2\nu_n\gamma_p - 2\delta_{np}\gamma_q\nu_q}{4\pi\rho\alpha^2 r^2}\right)\mu A \bar{u}_p\left(t - \frac{r}{\alpha}\right) \\
&\quad - \left(\frac{12\gamma_n\gamma_p\gamma_q\nu_q - 3\nu_n\gamma_p - 3\delta_{np}\gamma_q\nu_q}{4\pi\rho\beta^2 r^2}\right)\mu A \bar{u}_p\left(t - \frac{r}{\beta}\right) \\
&\quad + \frac{2\gamma_n\gamma_p\gamma_q\nu_q}{4\pi\rho\alpha^3 r}\mu A \dot{\bar{u}}_p\left(t - \frac{r}{\alpha}\right) - \left(\frac{2\gamma_n\gamma_p\gamma_q\nu_q - \nu_n\gamma_p - \delta_{np}\gamma_q\nu_q}{4\pi\rho\beta^3 r}\right)\mu A \dot{\bar{u}}_p\left(t - \frac{r}{\beta}\right).
\end{aligned}
\tag{4.30}
$$

Our next goal is to turn this expression, for the displacement field radiated by a shear dislocation, from its Cartesian form into a form that naturally brings out the radial and transverse components of motion. This goal can be accomplished by choosing axes so that the fault lies in the (x_1, x_2) plane, i.e., $\boldsymbol{\nu} = (0, 0, 1)$, with $\boldsymbol{\xi} = \mathbf{0}$, and introducing spherical polar coordinates r, θ, and ϕ centered on the source. We measure θ from the x_3-direction (see Fig. 4.4); choose the x_1-axis to be the direction of slip, so that $\bar{\mathbf{u}} = (\bar{u}, 0, 0)$; and take $\phi = 0$ as the plane containing $\boldsymbol{\nu}$ and $\bar{\mathbf{u}}$. Unit vectors $\hat{\mathbf{r}}, \hat{\boldsymbol{\theta}}, \hat{\boldsymbol{\phi}}$ are in the directions of r, θ, ϕ increasing (respectively) so that the "radial" direction is along $\hat{\mathbf{r}}$, and $\hat{\boldsymbol{\theta}}$ and $\hat{\boldsymbol{\phi}}$ are both "transverse" directions.

We seek to express the displacement vector at $\mathbf{x}$, for which the nth Cartesian component is given in (4.30), as a sum of vectors in the three directions $\hat{\mathbf{r}}, \hat{\boldsymbol{\theta}}$, and $\hat{\boldsymbol{\phi}}$. Fortunately, (4.30) is composed of vectors of only three types—namely, $\gamma_n\gamma_p\bar{u}_p\gamma_q\nu_q$, $\nu_n\gamma_p\bar{u}_p$, and $\delta_{np}\bar{u}_p\gamma_q\nu_q$. These three types can be recognized, respectively, as follows:

$$
\begin{aligned}
2\gamma_n\gamma_p\bar{u}_p\gamma_q\nu_q \quad &\text{is the } n\text{th component of } \bar{u}\ \sin 2\theta \cos\phi\ \hat{\mathbf{r}}, \\
2\nu_n\gamma_p\bar{u}_p \quad &\text{is the } n\text{th component of } \bar{u}\ \sin 2\theta \cos\phi\ \hat{\mathbf{r}} - \bar{u}\, 2\sin^2\theta \cos\phi\ \hat{\boldsymbol{\theta}}, \\
2\delta_{np}\bar{u}_p\gamma_q\nu_q \quad &\text{is the } n\text{th component of } \bar{u}\ \sin 2\theta \cos\phi\ \hat{\mathbf{r}} + \bar{u}\, 2\cos^2\theta \cos\phi\ \hat{\boldsymbol{\theta}} \\
&\qquad - \bar{u}\, 2\cos\theta \sin\phi\ \hat{\boldsymbol{\phi}}.
\end{aligned}
\tag{4.31}
$$

These results follow from relations $\hat{\mathbf{r}} = \boldsymbol{\gamma} = (\sin\theta\cos\phi, \sin\theta\sin\phi, \cos\theta)$, $\hat{\boldsymbol{\theta}} = (\cos\theta\cos\phi, \cos\theta\sin\phi, -\sin\theta)$, and $\hat{\boldsymbol{\phi}} = (-\sin\phi, \cos\phi, 0)$.

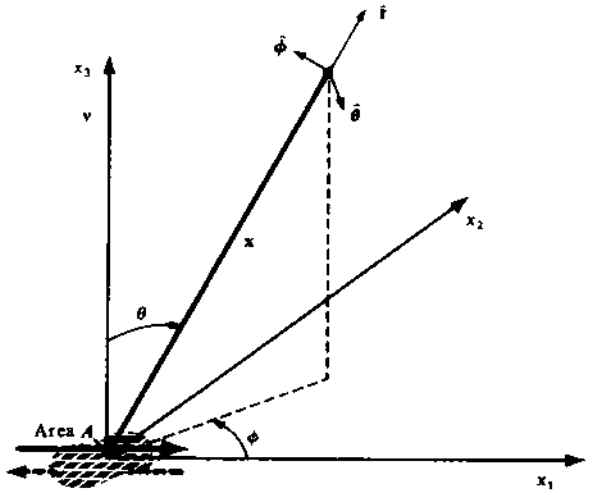

FIGURE **4.4**
Cartesian and spherical polar coordinates for analysis of radial and transverse components of displacement radiated by a shear dislocation of area A and average slip $\bar{u}$. See (4.31).

With the identification of vector components in (4.31), it now becomes possible to write our displacement field $u_n = M_{pq} * G_{np,q}$ in a concise vector form, using the time-dependent seismic moment $M_0(t) = \mu\bar{u}(t)A$. We find

$$\begin{aligned}\mathbf{u}(\mathbf{x},t) = {} & \frac{1}{4\pi\rho}\mathbf{A}^N\frac{1}{r^4}\int_{r/\alpha}^{r/\beta}\tau M_0(t-\tau)\,d\tau \\ & + \frac{1}{4\pi\rho\alpha^2}\mathbf{A}^{IP}\frac{1}{r^2}M_0\left(t-\frac{r}{\alpha}\right) + \frac{1}{4\pi\rho\beta^2}\mathbf{A}^{IS}\frac{1}{r^2}M_0\left(t-\frac{r}{\beta}\right) \\ & + \frac{1}{4\pi\rho\alpha^3}\mathbf{A}^{FP}\frac{1}{r}\dot{M}_0\left(t-\frac{r}{\alpha}\right) + \frac{1}{4\pi\rho\beta^3}\mathbf{A}^{FS}\frac{1}{r}\dot{M}_0\left(t-\frac{r}{\beta}\right),\end{aligned} \tag{4.32}$$

in which the near-field, the intermediate-field P and S, and the far-field P and S have radiation patterns given, respectively, by

$$\begin{aligned}\mathbf{A}^N &= 9\sin 2\theta\cos\phi\,\hat{\mathbf{r}} - 6(\cos 2\theta\cos\phi\,\hat{\boldsymbol{\theta}} - \cos\theta\sin\phi\,\hat{\boldsymbol{\phi}}) \\ \mathbf{A}^{IP} &= 4\sin 2\theta\cos\phi\,\hat{\mathbf{r}} - 2(\cos 2\theta\cos\phi\,\hat{\boldsymbol{\theta}} - \cos\theta\sin\phi\,\hat{\boldsymbol{\phi}}) \\ \mathbf{A}^{IS} &= -3\sin 2\theta\cos\phi\,\hat{\mathbf{r}} + 3(\cos 2\theta\cos\phi\,\hat{\boldsymbol{\theta}} - \cos\theta\sin\phi\,\hat{\boldsymbol{\phi}}) \\ \mathbf{A}^{FP} &= \sin 2\theta\cos\phi\,\hat{\mathbf{r}} \\ \mathbf{A}^{FS} &= \cos 2\theta\cos\phi\,\hat{\boldsymbol{\theta}} - \cos\theta\sin\phi\,\hat{\boldsymbol{\phi}}.\end{aligned} \tag{4.33}$$

These radiation patterns explicitly display a radial component, proportional to $\sin 2\theta\cos\phi\,\hat{\mathbf{r}}$, and a transverse component, proportional to $(\cos 2\theta\cos\phi\,\hat{\boldsymbol{\theta}} - \cos\theta\sin\phi\,\hat{\boldsymbol{\phi}})$. The important property brought out by (4.33) is that these are the only two radiation patterns needed to obtain a complete picture of all the different terms in the displacement field radiated from a shear dislocation (double couple). Figure 4.5 shows the way in which

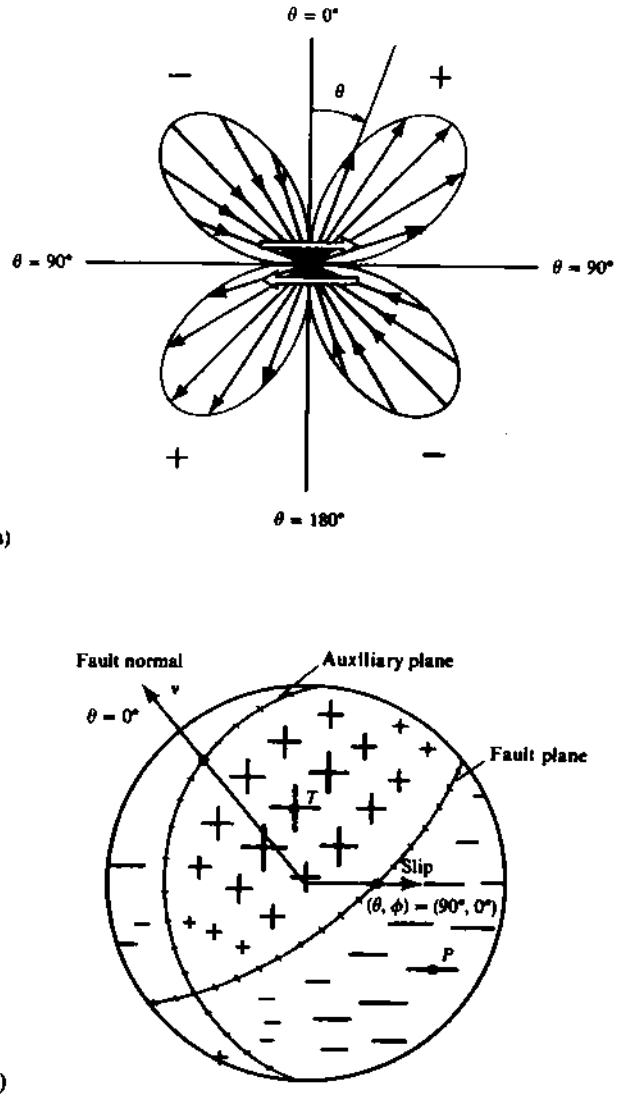

FIGURE 4.5
Diagrams for the radiation pattern of the radial component of displacement due to a double couple, i.e., $\sin 2\theta \cos\phi\, \hat{\mathbf{r}}$. (a) The lobes are a locus of points having a distance from the origin that is proportional to $\sin 2\theta$. The diagram is for a plane of constant azimuth, and the pair of arrows at the center denotes the shear dislocation. Note the alternating quadrants of inward and outward directions. In terms of far-field P-wave displacement, plus signs denote outward displacement (if $\dot{M}_0(t - r/\alpha)$ is positive), and minus signs denote inward displacement. (b) View of the radiation pattern over a sphere centered on the origin. Plus and minus signs of various sizes denote variation (with θ, ϕ) of outward and inward motions. The fault plane and the auxiliary plane are nodal lines (on which $\sin 2\theta \cos\phi = 0$). An equal-area projection has been used (see Fig. 4.17). Point P marks the pressure axis, and T the tension axis.

the radial component varies in magnitude for different directions (θ, ϕ), and Figure 4.6 shows how the transverse component varies in both magnitude and direction. Only the radial component is present for the far-field P-wave, and only the transverse component is present for the far-field S-wave. However, the intermediate-field displacements, both P and S, involve both radial and transverse components, as does the near-field displacement.

The surprisingly simple dependence on (θ, ϕ), which we have found in (4.32) and (4.33) and shown in Figures 4.5 and 4.6, prompts one to ask if a more direct method can be used in the derivation. Indeed this is the case, vector surface harmonics (see Chapter 8) providing the necessary analytical framework and demonstrating the simple dependence on (θ, ϕ) from the outset, but the associated algebraic manipulations for this more sophisticated method are

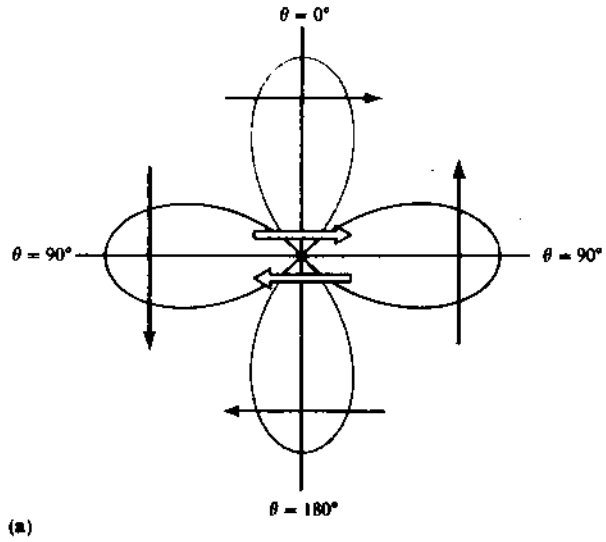

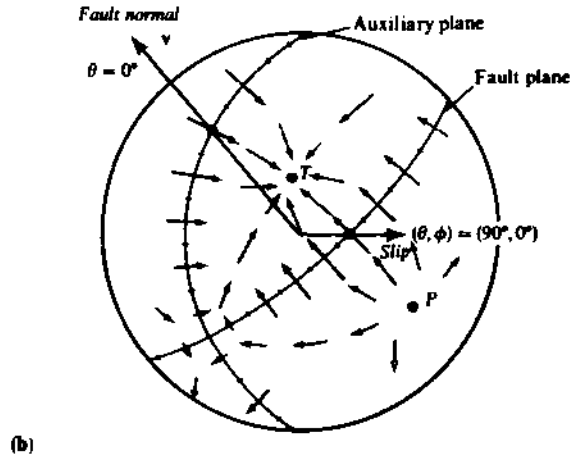

FIGURE 4.6

Diagrams for the radiation pattern of the transverse component of displacement due to a double couple, i.e., $\cos 2\theta \cos\phi\,\hat{\theta} - \cos\theta \sin\phi\,\hat{\phi}$. (a) The four-lobed pattern in plane $\{\phi = 0, \phi = \pi\}$. The central pair of arrows shows the sense of shear dislocation, and arrows imposed on each lobe show the direction of particle displacement associated with the lobe. If applied to the far-field S-wave displacement, it is assumed that $\dot{M}_0(t - r/\beta)$ is positive. (b) Off the two planes $\theta = \pi/2$ and $\{\phi = 0, \phi = \pi\}$, the $\hat{\phi}$ component is nonzero, hence (a) is of limited use. This diagram is a view of the radiation pattern over a whole sphere centered on the origin, and arrows (with varying size and direction) in the spherical surface denote the variation (with θ, ϕ) of the transverse motions. There are no nodal lines (where there is zero motion), but nodal points do occur. Note that the nodal point for transverse motion at $(\theta, \phi) = (45°, 0)$ is a maximum in the radiation pattern for longitudinal motion (Fig. 4.5b). But the maximum transverse motion (e.g., at $\theta = 0$) occurs on a nodal line for the longitudinal motion. The stereographic projection has been used (see Fig. 4.16). It is a conformal projection, meaning that it preserves the angles at which curves intersect and the shapes of small regions, but it does not preserve relative areas.

(in our opinion) as laborious as the Cartesian analysis we have chosen to use. In Section 4.4, we shall develop properties of the far-field displacement for a medium that, like the Earth, is inhomogeneous. In Section 4.5 we shall reexamine the radiation patterns (4.33), showing how they may be used in practice to obtain (from seismic data) the fault-plane orientation and the direction of slip.

To conclude the present section, we obtain from (4.32) the final static displacement field for a shear dislocation of strength M_0. This involves taking the limit of $\dot{M}_0(t-\tau)$, $M_0(t-\tau)$, and $\int_{r/\alpha}^{r/\beta} \tau M_0(t-\tau)\, d\tau$ as $t \to \infty$, assuming that the seismic moment itself has a final constant value, $M_0(\infty)$. The result is

$$\begin{aligned}\mathbf{u}(\mathbf{x},\infty) &= \frac{M_0(\infty)}{4\pi\rho r^2}\left[\mathbf{A}^N\left(\frac{1}{2\beta^2}-\frac{1}{2\alpha^2}\right)+\frac{\mathbf{A}^{IP}}{\alpha^2}+\frac{\mathbf{A}^{IS}}{\beta^2}\right] \\ &= \frac{M_0(\infty)}{4\pi\rho r^2}\left[\frac{1}{2}\left(\frac{3}{\beta^2}-\frac{1}{\alpha^2}\right)\sin 2\theta\cos\phi\,\hat{\mathbf{r}}\right. \\ &\qquad \left. +\frac{1}{\alpha^2}(\cos 2\theta\cos\phi\,\hat{\boldsymbol{\theta}}-\cos\theta\sin\phi\,\hat{\boldsymbol{\phi}})\right],\end{aligned} \tag{4.34}$$

which attenuates (along any given direction (θ,ϕ)) as r^{-2}.

4.4 Ray Theory for Far-Field *P*-waves and *S*-waves from a Point Source

Books and papers on the theory of elastic wave propagation are for the most part concerned with homogeneous media. Seismologists often require a good grasp of the properties of waves in such simple media and of the exact solutions that may be obtained (e.g., Chapters 5 and 6). However, the practical analysis of seismograms requires also a good grasp of approximate solutions for the waves that propagate in inhomogeneous media. Not only does the Earth have material boundaries across which the elastic properties are discontinuous, but also it contains vast regions within which there is a systematic and continuous change of bulk modulus, rigidity, and density. Thus P-wave and S-wave velocities both increase by a factor of about two from the top to the bottom of the mantle, and this is enough to distort beyond recognition the radiation patterns we have described above, unless the effects of inhomogeneity are accounted for. In this section and the next, we show how to remove the distortion, and demonstrate how amplitudes of body waves can be substantially changed by focusing or defocusing effects of the type exhibited by light propagating in media of varying refractive index. The approximate solution we shall obtain, called the geometric ray solution, provides a guide to more sophisticated methods, should they be necessary.

Ray theory can perhaps best be remembered as a collection of verifiable intuitive ideas and approximations. Thus body waves travel with a local propagation speed along "ray paths" determined by Snell's law, arriving (as a "wavefront") with an amplitude determined by the geometrical spreading of rays from the source to the receiver. These are statements that we shall prove, but intuition enters strongly at the initial stage of setting up a trial form for the solution.